ACS Biomaterials SCIENCE & ENGINEERING

pubs.acs.org/journal/abseba

Article

Detection of Leptin Using Electrocatalyst Mediated Impedimetric Sensing

Tamanna Islam,[♦] Md Ariful Ahsan,[♦] Masud Hassan, Humayra Afrin, Jaqueline Pena-Zacarias, Ali Aldalbahi, Bonifacio Alvarado-Tenorio, Juan C. Noveron,* and Md Nurunnabi*

Cite This: https://doi.org/10.1021/acsbiomaterials.2c00642

Read Online

ACCESS | Metrics & More | Article Recommendations | Supporting Information

ABSTRACT: Obesity is a complex disorder associated with immense health consequences including high risk of cardiovascular diseases, diabetes, and cancer. Abnormality in the thyroid gland, genetics, less physical activity, uptake of excessive diet, and leptin resistance are critical factors in the development of obesity. To determine the treatment strategy, understanding the pathophysiology of obesity is crucial. For instances, leptin resistance mediated obesity defined by the presence of excessive leptin hormone (Lep) in the systemic circulation is very common in diet induced obesity. Therefore, our hypothesis is that quantitative measurement of Lep from blood can help to identify individuals with Lep resistant mediated obesity and thereby guide toward a proper treatment strategy. In this work, we aim to utilize an electrochemical immunosensing platform for diagnosis of obesity by measuring the Lep content in systemic circulation. A porous carbon confined FeNi bimetallic system was synthesized with three different ratios of Fe and Ni ions using high temperature pyrolysis technique. The suitability of the sensor for detecting Lep was studied using both CV and EIS techniques. The limit of detection (LOD) for GCE was recorded as 157.4 fg/mL with a wide linear concentration range of 500 fg/mL to 80 ng/mL, while for SPCE the LOD was 184.9 fg/mL with a linear range of 500 fg/mL to 50 ng/mL. Finally, the feasibility and applicability of the sensor for Lep detection was tested with serum collected from high fat diet induced obese rats. The selectivity, sensitivity, storage, and experimental stability and reproducibility tests showed potential for this biosensor platform as a point-of-care Lep detection device.

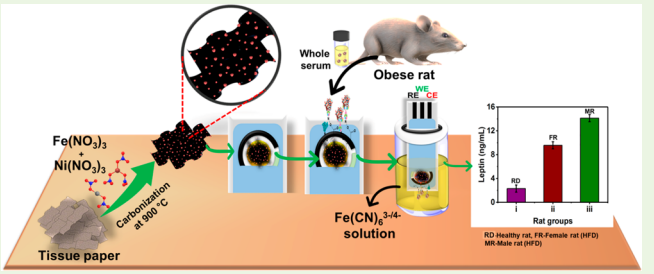

KEYWORDS: *Obesity, Leptin detection, Immunosensor, Screen printed carbon electrode, Point-of-care*

1. INTRODUCTION

The world has seen an exponential rise of severe obesity in both adults and children in recent years, making it a public health crisis.[1−3] The recent Behavioral Risk Factor Surveillance System (BRFSS) data showed that the adult obesity rate has increased by 35% in almost 16 states in the U.S. Obesity is one of the key reasons for abnormalities in lipid and glucose metabolism.[4] Thereby, obesity is very closely linked with diabetes (types 1 and 2) and cardiovascular diseases.[3] Obesityis also responsible for various cancers and arthritis. Moreover, recent studies have shown that obese COVID-19 patients are more likely to have severe conditions and a higher death count.[1,2,5−7] Therefore, it is imperative to identify obesity markers at an earlier stage in order to prevent obesity related complications and diseases. Lep is an adipose tissue secreted (16-kDa) protein hormone synthesized by the ob gene that regulates mammalian appetite through the body's energy status.[8,9] Lep controls the nutritional needs of the body by interacting with the hypothalamus.[8,10] Lep concentration in humans varies with sex, age, and genetic abnormality.[9,11] The normal blood concentration of Lep in males and females is ∼11.1 and ∼5.6 ng/mL, respectively.[11] However, those with obese conditions can have a Lep concentration of ∼100 ng/mL, and Lep gene abnormalities can result in 300−700 ng/mL concentration.[11,12] A slight increase of Lep would usually lead to a reduction of the appetite and, hence, helps maintain body mass. However, under obese conditions, although adipose tissue produces copious amounts of Lep in the body, the potentiality of Lep to show an anorexic effect on the brain is reduced. It is a situation termed "leptin resistance" where Lep signaling in the hypothalamus region of the brain gets disrupted due to the blockage of intracellular signaling associated with impaired Lep receptors or a lowering of Lep transportation through the blood brain barrier (BBB).[13] Because of its huge significance in obesity progression, leptin resistance is now believed to be one of the key parameters for diagnosing obesity. As Lep is an important biomarker of

Special Issue: Bioinspired Materials for Wearable Diagnostics and Biosensors

Received: June 4, 2022
Accepted: September 12, 2022

obesity, it is imperative to develop highly effective sensors that will be able to detect Lep in a physiological concentration from real samples with high precision.

The most widely used methods for Lep detection include radioimmunoassay, SPR, enzyme-linked immunoassay (ELISA), capillary electrophoresis, and electrochemical biosensors (ECBs).[8−10,14,15] High sensitivity, good anti-interference ability, ease of sample preparation and operation, and cost-effectiveness are the key benefits of ECBs.[16] Among different kinds of ECBs, the immunosensors are advantageous as they can selectively detect specific analytes through bioaffinity.[16] One of the key areas of improvement for immunosensors is the development of highly electroactive and biocompatible catalytic materials.[17] Lep has a quaternary structure with an active disulfide bond.[11,12] This structure or the active site can be exploited for highly efficient detection of Lep. Due to clinical potential, various metallic, graphene, porous carbon, and polymer based catalytic systems were utilized for enhancing the sensitivity of the immunosensors for Lep detection.[8,14,18,19]

Metallic nanoparticles embedded within porous carbon structures have shown very good electrocatalytic activity in diverse areas of electrochemical research.[19−22] Those with a heterometallic system are more promising as electrocatalysts compared to their monometallic counterparts.[23] The cations of the heterometallic systems are chosen to facilitate compatibility of the metal ions with each other. The metallic $\pi-\pi$ interactions lead to a synergetic increase in their electrocatalytic activity, while the carbon base provides support that stabilizes the metallic nanoparticle. Previous reports have shown that both Fe and Ni have excellent electrocatalytic activity, and when combined together they show synergistic interaction.[18,21−24]

In this publication, we report on the preparation of an impedimetric sensor for diagnosing leptin resistance based on three heterometallic FeNi/C systems having different metallic ratios with excellent biocompatibility and conductivity. The morphological properties, degree of defects, chemical composition, functional groups, and electrochemical properties of the materials were investigated, and the suitability of each of the three electrocatalysts for biomolecule immobilization and subsequent sensing feasibility were assessed. As per the analysis, the Fe:Ni(1:1)/C system provided superior efficacy for anti-Lep immobilization and further immuno-conjugation. The binding affinity of anti-Lep with the electrocatalyst was further confirmed through surface plasmon resonance (SPR) sensogram analysis. Upon determination of the most effective material for Lep detection, we utilized the LepSens (leptin sensor) for the detection of Lep over a concentration window using both glassy carbon electrodes (GCEs) and screen-printed carbon electrodes (SPCEs). After laboratory data acquisition, the sensor was implemented for serum analysis collected from a set of obese rats, induced by a high fat diet, which demonstrated excellent outputs comparable with the laboratory analysis. The stability, performance, reproducibility, and selectivity of the LepSens were further studied to determine the adequacy and potency of the sensor. With further validation and optimization of the sensor by utilizing patient derived serum samples, the LepSens has strong potential for clinical translation for real-time diagnosis of leptin resistance in obesity.

2. MATERIALS AND METHODS

2.1. Materials. Iron nitrate ($Fe(NO_3)_3{\cdot}6H_2O$) and nickel nitrate ($Ni(NO_3)_2{\cdot}6H_2O$) were purchased from Sigma-Aldrich. Deionized water (DIW) was used from a Milli-Q instrument (Millipore Corporation). Tissue paper was purchased from a local store. Biomolecules used in this work such as recombinant human Lep protein, anti-Lep (polyclonal, pAb), interleukin-6 (IL 6), troponin I_3 (TnI_3), and vascular cell adhesion protein1 (VCAM1) were purchased from ABclonal Science Inc. (Woburn, MA). Bovine serum albumin (BSA), potassium ferricyanide ($K_3Fe(CN)_6$), mono and dibasic potassium phosphate (KH_2PO_4 and K_2HPO_4), potassium chloride (KCl), and glucose were purchased from Thermo Fisher Scientific Inc. N-(3-(Dimethylamino)propyl)-N-ethylcarbodiimide hydrochloride (EDC·HCl), and *N*-hydroxysuccinimide (NHS) were purchased from Sigma Aldrich, USA. All experiments were carried out using distilled water (electrolytes concentration-1.3 ppb). For electrochemical sample preparation, all biomolecules' solutions were prepared in 0.1 M phosphate buffer saline (PBS) solution. A 5 mM concentrated $K_3Fe(CN)_6$ solution was used in all electrochemical experiments and was prepared by dissolving it in 1.0 M KCl solution. The PBS solution of concentration 0.1 M was prepared by mixing KH_2PO_4 and K_2HPO_4 in distilled water.

2.2. Synthesis of the Electrocatalysts. Initially, 1.5 g of each metal salt was dissolved in 10 mL of DIW in a 100 mL beaker. Subsequently, 3.0 g of facial tissue (in the form of tiny pieces) was placed into the metal salt solution, and the bimixture was sonicated so that the Fe^{3+} and Ni^{2+} ions were adsorbed on the facial tissue, followed by heating the mixture at 100 °C to remove all of the water molecules. Afterward, the mixture was carbonized at 800 °C for 4 h in a tube furnace, and the heating rate was set to 5 °C min^{-1}. The black product of bimetallic nanoparticles was collected and named Fe:Ni(1:1)/C. Another two bimetallic electrocatalysts, namely, Fe:Ni(3:1)/C and Fe:Ni(1:3)/C, were prepared with respect to different weight ratios of the iron and nickel salts that were used during the synthesis process.

2.3. Electrode Modification and Optimization Process. The electrochemical sensor was constructed by following a layer-by-layer modification process. At first, the GCE was polished with a 0.05 μm alumina slurry for 30 min to remove any adsorbed oxide layers. Then, the electrode was washed three times with distilled water and dried at room temperature. A value of 3 μL of the nanomaterial suspension (in methanol, 5 mg/mL) was drop-casted on the electrode surface and dried in air. Once the electrode surface was dried, a mixture of 10 mg/mL of EDC·HCl and 6 mg/mL of NHS was immobilized on the electrode surface by incubating in the EDC-NHS solution for 30 min. The EDC/NHS solution is a well-known cross-linker which is capable to initiate an active end that can efficiently bind with the $-NH_2$ group of the antibody by creating a −CO−NH− linkage. The EDC-NHS/FeNi/C_GCE electrode was then immobilized in the anti-Lep solution to prepare an antibody modified electrode. To block any nonspecific binding sites on the electrode surface, the modified was incubated in a 0.5% BSA solution. The final electrode was termed BSA/anti-Lep/EDC-NHS/FeNi/C_GCE and stored at 4 °C until use. Before conducting an electrochemical experiment, the electrode was incubated in the Lep solution and dried at 4 °C. The same procedure was further followed for constructing an SPCE based Lep biosensor. The electrode incubation times in different solutions, especially in the anti-Lep, BSA, and Lep solutions, were optimized by observing the changes in the EIS signals after incubating electrodes in different time periods (30, 45, 60, and 90 min). It is worth noting that the electrode was kept at 4 °C while incubating in different biomolecular solutions for different time periods and washed carefully with distilled water after each modification to ensure complete removal of any substances that were not bound to the electrode. All biorecognition molecules were diluted in 0.1 M PBS solution.

2.4. Instrumentations. To fabricate the LepSens, the bimetallic FeNi nanoparticles were first characterized using X-ray diffraction (XRD) spectroscopy with a Cu Kα radiation source in 2θ = 20−80° at a scan rate of 5 °C min^{-1} (Model: Bruker D8 advanced

https://doi.org/10.1021/acsbiomaterials.2c00642
ACS Biomater. Sci. Eng. XXXX, XXX, XXX−XXX

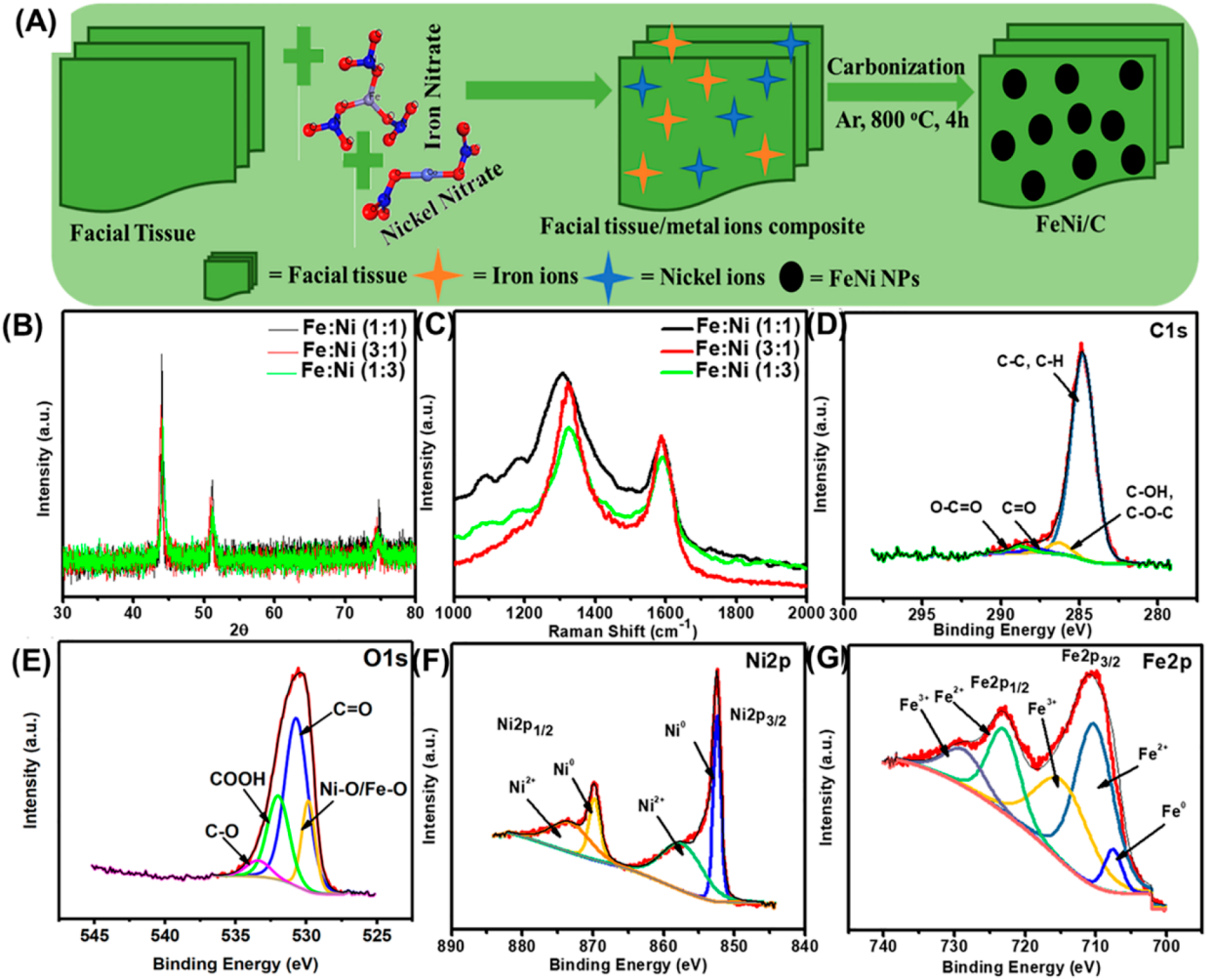

Figure 1. (A) Synthetic strategy, (B) XRD pattern, and (C) Raman spectra of FeNi/C nanocomposite and (D−G) high resolution XPS spectra of C 1s, O 1s, Ni 2p, and Fe 2p, respectively, of the Fe:Ni(1:1)/C nanocomposite.

diffractometer). Transmission electron microscopic (TEM) analysis was carried out on a Hitachi H-7650 microscope to further inspect the morphology of the nanoparticles. The surface elements and chemical valence of the nanoparticles were detected using X-ray photoelectron spectroscopy (XPS) on a PHI VersaProbe II Scanning XPS Microprobe with scanning monochromatic X-ray Al Kα radiation as the excitation source (200 μm area analyzed, 52.8 W, 15 kV, 1486.6 eV) and a charge neutralizer. For a biomolecule−electrocatalyst binding affinity study, an iMSPR instrument was used (iCLUEBiO Co. Ltd., Republic of Korea). The carboxylated Au chips used for the SPR analysis were also purchased from iCLUEBiO Co. Ltd. All electrochemical experiments, namely, electrochemical impedance spectroscopy (EIS) and cyclic voltammetry (CV) were performed using an CHI660E electrochemical workstation, CHI Inc., USA. A three electrode setup was utilized where both classical GCE and SPCE were used as the working electrode, Ag/AgCl as the reference, and Pt wire as the counter electrode and were purchased from CHI Inc., USA.

2.5. Obese Rat Model and Serum Sample Preparation for Lep Detection. Six Sprague−Dawley rats (male/female) were chosen for preparing the obese rat model. All experiments were performed after approval from the Institutional Animal Care and Use Committee (IACUC) of the University of Texas at El Paso (Protocol no. A-201910-1). The rats were fed a high fat diet (HFD, extra 60% calories) for 15 days to induce obesity through observing the changes in their body weight every day. For comparison, another group of six rats were considered which were given a regular diet (RD, 10% calories) every day. After creating the obese rat model, both RD and HFD rats were sacrificed, and the blood sample was collected. The blood was centrifuged at 1500 rpm for 10 min to separate the serum. For electrochemical measurements, the serum samples of the RD rats were first diluted 50 times in normal PBS and spiked with two different concentrations of Lep (500 pg/mL and 1 ng/mL), while the serum of the HFD rats was directly used without any spiking procedures. For constructing the modified electrodes, the same layer-by-layer modification process was followed. The final modified electrode was incubated in diluted spiked serum (RD)/whole serum (HFD) for Lep quantification.

2.6. Electrochemical Measurements. For electrochemical characterization of the FeNi bimetallic system and Lep signaling, both CV and EIS techniques were utilized. To evaluate the conjugation of the biomolecules with the sensor, the changes in the redox peak responses of potassium ferricyanide at the electrode−electrolyte interface were investigated, which was achieved by taking the solution of $K_3Fe(CN)_6$ in the electrochemical cell. The frequency range used for EIS analysis was 1 Hz (low) to 1 MHz (high), and the initial potential was chosen based on the formal potential of potassium ferricyanides obtained by averaging the oxidation and reduction peak potentials from the CV experiment. Averaging was done following eq 1:

$$E_f = \frac{E_{pa} + E_{pc}}{2} \quad (1)$$

https://doi.org/10.1021/acsbiomaterials.2c00642
ACS Biomater. Sci. Eng. XXXX, XXX, XXX−XXX

2.7. Methods for Validating Sensors' Applicability. To evaluate the applicability of the proposed sensor, we performed a quantitative analysis of Lep by using the EIS technique over a wide concentration range. The value of charge transfer resistance (R_{ct}) was determined for each of the EIS data and plotted against the concentration of Lep (calibration plot). By using the intercept and slope of the calibration plot, the LOD, sensitivity, and linear range of the sensor for Lep were determined following eq 2.

$$\mathrm{LOD} = \frac{3.3 \times \mathrm{SE}}{s} \quad (2)$$

where SE refers to the standard deviation and s to the slope of the calibration plot.

The selectivity, sensitivity, and specificity of the sensor were evaluated by performing interference analysis. A variety of biomolecules that are expected to be present in the serum sample were used in which the modified electrode was incubated to see whether the sensor shows any affinity toward those biomolecules. The percentages of R_{ct} obtained for incubating the modified electrodes in the interfering agents were compared with the value of R_{ct} obtained for Lep only. While on the other hand, for evaluating the sensitivity and the specificity of the sensor, a mixture of Lep and the interfering agents was used where the modified electrode was incubated. Once the sensor selectively bound with Lep from the mixture, the EIS experiment was carried out and the standard deviation in the obtained EIS signal was evaluated with respect to the response obtained for Lep only to determine the sensitivity and the specificity of the sensor. To test the sensor's applicability in detecting Lep from a real sample, the serum of the RD/HFD rats was separated and prepared as described in the previous section. For assessing the performance of the sensor, the signal stability, storage stability, and the reproducibility of the EIS signal regardless of the number of electrodes were investigated. For these purposes, consecutive EIS analysis, signal acquisition of the modified electrode after more than a week, and EIS of six different GCE electrodes were performed.

2.8. Software and Simulation. The latest version of CHI 660E was used for electrochemical experiments. The modified Randle's circuit fitting was also done with the CHI 660E software. CasaXPS was used for analyzing the results from the XPS experiment. All experimental data were plotted with the Origin 2017 software.

3. RESULTS AND DISCUSSION

3.1. Structural Characterization. The synthesis process of the FeNi/C nanohybrid is presented in Figure 1A. As seen, the synthesis of the FeNi/C nanocomposite electrocatalyst was accomplished via a two-step strategy that includes the adsorption of the Ni^{2+}/Fe^{3+} ions into facial tissue followed by pyrolysis.[20] During the pyrolysis step, the facial tissue serves as a carbon source, while the metal salts acted as a metal source, to form the final carbon encapsulated FeNi structure. The crystalline structure of the bimetallic NPs was first investigated using XRD, as shown in Figure 1B. The XRD pattern showed three characteristic diffraction peaks in all cases at ~44.22°, 51.25°, and 74.89°. These peaks correspond to the 111, 200, and 220 crystal planes of the cubic FeNi alloy (JCPDS no. 65−3244), confirming the successful formation of the FeNi nanocomposite.[22] The diffraction pattern did not show any additional peaks, suggesting the high purity of the as-prepared FeNi alloy.

Raman spectroscopic analysis was further performed for investigating the structural distinction of as-prepared FeNi/C nanoelectrocatalysts (Figure 1C). As seen from this figure, mainly two typical peaks can be distinctly identified at ~1339 and 1590 cm^{-1} for all of the samples, assigned to the D and G bands, respectively.[20,22] The D band is associated with a breathing mode of κ-point photons of A_{1g} symmetry, while the G band arises from the first order scattering of the E_{2g} phonon of sp^2-banded carbon atoms. The intensity ratio of these two bands (I_D/I_G) is sensitive to the disorder degree, and its increasing value manifests the formation of defects. As seen in this figure, the I_D/I_G values of the as prepared three nanohybrids are higher than one. It indicates that a higher degree of defects is introduced into the composites during the bimetallic nanoelectrocatalyst's formation, which is beneficial to improving the electrocatalytic properties.[20]

XPS analysis was further performed to examine the valence states and chemical composition of the FeNi/C nanocomposite. The survey scan of the XPS spectra showed the presence of carbon, oxygen, iron, and nickel elements in the Fe:Ni(1:1)/C nano electrocatalyst sample (Figure S1). The high resolution C 1s spectra in Figure 1D was deconvoluted into four bands that corresponds to C−O−C/C−OH, C−C/C−H, C═O, and O−C═O.[24,25]

The O 1s peak was deconvoluted into four peaks that correspond to the Ni−O/Fe−O, C−O, C═O, and −COOH (Figure 1E).[24,26] The existence of the oxygenated functional groups might provide more nucleation sites to favor the growth of the bimetallic nanocomposites.[22] As seen in Figure 1F, the Ni 2p band primarily comprises Ni $2p_{1/2}$ and Ni $2p_{3/2}$; each of them was then fitted into two peaks corresponding to the Ni^0 and Ni^{2+}. The Ni^{2+} peak usually corresponds to the nickel oxide. This could happen because of the air exposure, which might favor the formation of a thin layer of metal oxide as the Ni NPs are air sensitive.[23,27,28] Likewise, the Fe 2p band also mainly consists of Fe $2p_{1/2}$ and Fe $2p_{3/2}$ (Figure 1G). They were fitted into three peaks that correspond to Fe^0, Fe^{2+}, and Fe^{3+}.[29,30] Therefore, the presence of metallic iron and nickel in the FeNi/C demonstrates the successful synthesis of FeNi bimetallic nanocomposites. Then, the morphology of the nanocomposite was inspected using transmission electron microscopic analysis. As seen in Figure 2A−C, the FeNi bimetallic NPs are uniformly dispersed and anchored into the porous carbon framework in case of all of the FeNi bimetallic nanocomposites. Hence, the porous carbon framework plays a dual role being a substrate and protecting layer for the bimetallic NPs and protect them from further oxidation. The average particle size of the nanocomposite was found to be ~15−20 nm in diameter. Furthermore, the energy dispersive X-ray spectroscopy (EDS) elemental color mapping experiments of the Fe:Ni(1:1)/C nanocomposite showed the presence of all of the expected elements such as carbon, oxygen, nickel, and iron, as seen in Figure 2D−G.

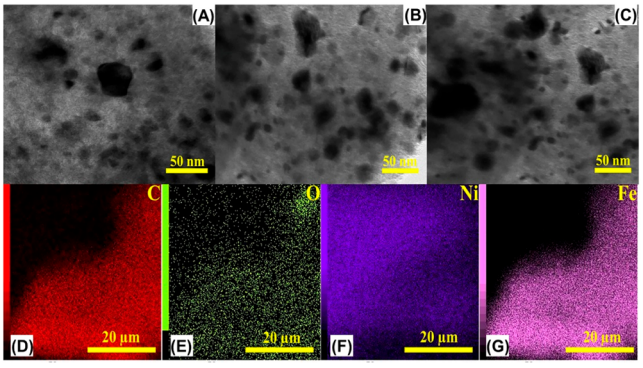

Figure 2. (A−C) TEM images of Fe:Ni(1:1)/C, Fe:Ni(3:1)/C, and Fe:Ni(1:3)/C nanocomposites, respectively, and (D−G) EDS elemental color mapping of the Fe:Ni(1:1)/C nanocomposite.

https://doi.org/10.1021/acsbiomaterials.2c00642
ACS Biomater. Sci. Eng. XXXX, XXX, XXX−XXX

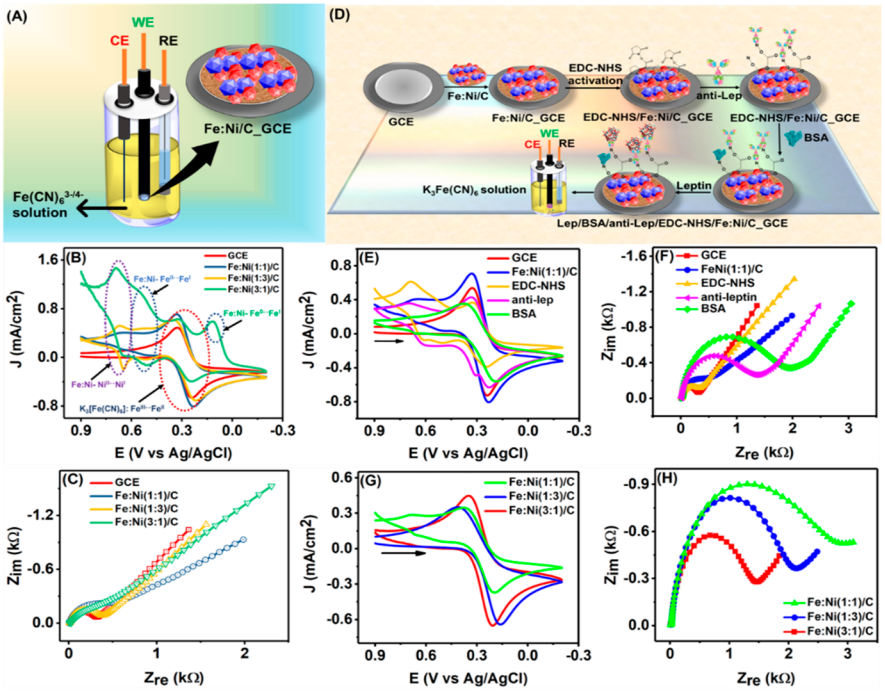

Figure 3. Electrochemical characterization and electrochemical behavior of the FeNi/C nanocomposite toward Lep detection with 5 mM $K_3[Fe(CN)_6]$ in 1.0 M KCl solution. (A) Schematic presentation of the three electrodes setup for electrochemical characterization of the FeNi/C composite modified GCE. (B) CV of polished GCE, Fe:Ni(1:1)/C, Fe:Ni(1:3)/C, and Fe:Ni(3:1)/C nanocomposites. (C) EIS of polished GCE, Fe:Ni(1:1)/C, Fe:Ni(1:3)/C, and Fe:Ni(3:1)/C nanocomposites. (D) Schematic representation of the layer-by-layer modification of the GCE for Lep detection. (E) CV and (F) EIS data for sequential modification of the Fe:Ni(1:1)/C_GCE electrodes. (G) CV and (H) EIS plots for 500 pg/mL of Lep incubation for the Lep/BSA/anti-Lep/EDC-NHS/Fe:Ni(1:1)/C_GCE, Lep/BSA/anti-Lep/EDC-NHS/Fe:Ni(1:3)/C_GCE, and Lep/BSA/anti-Lep/EDC-NHS/Fe:Ni(3:1)/C_GCE.

3.2. Electrochemical Characterization of FeNi/C nanocomposite. The electrochemical properties of FeNi/C nanocomposites were analyzed using standard 5 mM $K_3[Fe(CN)_6]$ in 1.0 M KCl solution. The electrode setup and modification is shown in Figure 3A. Figure 3B and C reveal the CV and EIS plots obtained for polished GCE, Fe:Ni(1:1)/C, Fe:Ni(1:3)/C, and Fe:Ni(3:1)/C NPs. The CV plots (Figure 3A) showed distinguishing features for the different FeNi/C nanocomposites compared to polished GCE. The GCE showed redox peaks for $[Fe(CN)_6]^{3-} \leftrightarrow [Fe(CN)_6]^{4-}$ around 0.24 and 0.33 V (ΔE_p = 90 mV). The peak current densities (J) for the reduction and oxidation processes were determined to be −0.62 and 0.59 mA/cm^2, respectively. The 0.96 ratio of J_{pa}/J_{pc} and 90 mV ΔE_p shows that the $[Fe(CN)_6]^{3-/4-}$ redox process followed a reversible reaction pathway on the GCE. Once modified with the FeNi/C nanocomposites, the CV shape drastically changed, clearly indicating the surface modification of GCE. The Fe:Ni(1:1)/C_GCE, Fe:Ni(1:3)/C_GCE, and Fe:Ni(3:1)/C_GCE showed multiple redox peaks in their CV response. The individual CVs for GCE, Fe:Ni(1:1)/C_GCE, Fe:Ni(1:3)/C_GCE, and Fe:Ni(3:1)/C_GCE are shown in Figure S2 for clarity. In the case of Fe:Ni(1:1)/C_GCE, the redox pair for $[Fe(CN)_6]^{3-/4-}$ is observed around 0.23 (J_{pc} = −0.81 mA/cm^2) and 0.33 V (J_{pa} = 0.79 mA/cm^2). The Fe:Ni(1:3)/C_GCE had redox peaks around 0.22 (J_{pc} = −0.7 mA/cm^2) and 0.35 V (J_{pa} = 0.67 mA/cm^2), while the Fe:Ni(3:1)/C_GCE showed the redox peaks around 0.25 (J_{pc} = −0.42 mA/cm^2) and 0.32 V (J_{pa} = 0.48 mA/cm^2). The ΔE_p and J_{pa}/J_{pc} ratios for all three FeNi/C electrode systems are close to those for reversible redox systems. However, the Fe:Ni(1:1)/C_GCE had the highest J values. Indicating that the Fe:Ni(1:1)/C nanocomposite system was most active for the $K_3[Fe(CN)_6]$ redox process.

All three modified electrodes showed a weak signal for another redox pair around 0.5 V. This peak was for the $Fe^{2+/1+}$ oxidation states of the FeNi/C composite.[31,32] This can be clearly seen from the CV of Fe:Ni(3:1)/C_CGE, as it showed the highest J around 0.5 V. The peak pair around 0.65 V is likely for the $Ni^{1+/2+}$ of the FeNi nanocomposites.[33,34] The peak increased as the Ni ratio was increased in the Fe:Ni(1:3)/C nanocomposite. Aside from these, the Fe:Ni(3:1)/C showed another peak around 0.13 V. This peak is likely observed for the $Fe^{0/1+}$ oxidation process.[32,35] However, this peak is very unstable. As is seen from Figure S3, this peak decreases with each CV and ultimately disappears after the third consecutive CV. After that, the CV showed a steady response. This can be seen from the scan rate data of Figure S4. These CVs indicated that the high iron content of Fe:Ni(3:1)/C material is less stable compared to the other two. The consecutive CV analysis (50 CVs) as shown in Figure S5 also confirmed the stability of the Fe:Ni(1:1)/C over two other ratios, indicating its efficiency for biomolecule conjugation and immobilization. The scan rate variation data also show that the $K_3[Fe(CN)_6]$ redox process follows a diffusion controlled process for all three materials.

The experimental and fitted EIS data for the four electrodes are shown in Figure 3C. All of these electrode systems could be described using the modified Randle's circuit. The charge transfer resistances (R_{ct}) for the GCE, Fe:Ni(1:1)/C_GCE, Fe:Ni(1:3)/C_GCE, and Fe:Ni(3:1)/C_GCE were determined to be 245.1, 445.6, 324.2, and 223.4 Ω, respectively. These values indicate that Fe:Ni(3:1)/C material has the

https://doi.org/10.1021/acsbiomaterials.2c00642
ACS Biomater. Sci. Eng. XXXX, XXX, XXX−XXX

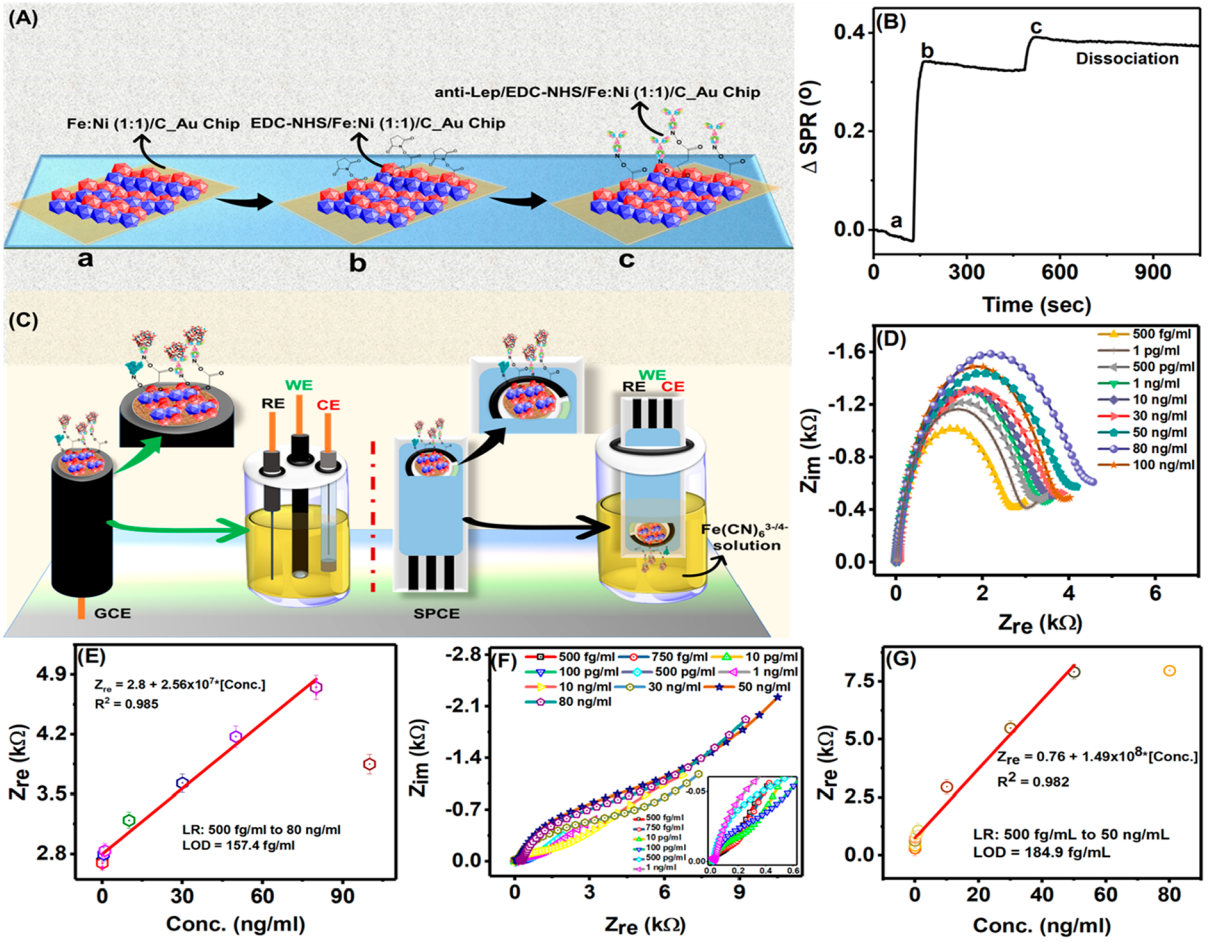

Figure 4. Study of the nanocomposite-anti-Lep binding affinity and quantitative detection of Lep with GCE and SPCE modified Fe:Ni(1:1)/C nanocomposite. (A) Scheme showing stepwise modification of a Au chip for an SPR based binding affinity study. (B) SPR sensorgram showing changes as EDC-NHS is injected (b) over the Fe:Ni(1:1)/C_Au and then corresponding changes in sensogram signal for injecting anti-Lep (c). (C) Schematic presentation of the electrode setup for quantitative detection of Lep with the Fe:Ni(1:1)/C_GCE and Fe:Ni(1:1)/C_SPCE. (D) Impedance signals observed at the Lep/BSA/anti-Lep/EDC-NHS/Fe:Ni(1:1)/C_GCE for the quantitative detection of Lep from 500 fg/mL to 100 ng/mL. (E) Calibration plot (R_{ct} vs concentration) showing the linear range for Lep with Fe:Ni(1:1)/C modified GCE. (F) Impedance signals observed at Lep/BSA/anti-Lep/EDC-NHS/Fe:Ni(1:1)/C_SPCE for the quantitative detection of Lep from 500 fg/mL to 80 ng/mL. (G) Calibration plot showing the linear range for Lep detection with Fe:Ni(1:1)/C modified SPCE.

lowest resistance to charge transfer for the $K_3[Fe(CN)_6]$, while Fe:Ni(1:1)/C material has the highest resistance. But the CV response showed the highest J value for the Fe:Ni(1:1)/C_GCE. The reason can be explained based on the charging current distribution. Compared to two other nanocomposites, Fe:Ni(1:1)/C shows a relatively low density of peaks other than the $[Fe(CN)_6]^{3-/4-}$ redox pair and hence low charging current, which could probably be responsible for the increment of R_{ct} for the Fe:Ni(1:1)/C nanocomposite. Also, the XPS data showed that, for the Fe:Ni/C nanocomposites, the partial negative charge containing groups ($-OH^{\delta-}$,$O^{\delta-}$,$O-C^{\delta-}$, etc.), these are very likely to repel the high negative charge bearing $[Fe(CN)_6]^{3-/4-}$, resulting in higher resistance to charge transfer.[36] The EDS data also indicated high negative functional group content on Fe:Ni(1:1)/C material. This high surface area would allow for more $[Fe(CN)_6]^{3-/4-}$ to interact with the Fe and Ni cations of the Fe:Ni(1:1)/C composite. The presence of functional groups and high surface area indicates that the Fe:Ni(1:1)/C could have good bonding with the immobilized antibodies for better Lep sensitivity.

3.3. Electrochemical Sensing of Lep. CV and EIS techniques were used for determining the potential of the Fe:Ni(1:1)/C, Fe:Ni(1:3)/C, and Fe:Ni(3:1)/C nanocomposite for Lep sensing. Figure 3D shows the step-by-step modification of the electrode for Lep detection. Figures 3E,F and S6A−D show the CV and EIS data for the step-by-step modification of the GCE using three different nanocomposites. The CV response increased after the initial modification with the Fe:Ni(1:1)/C material (Figure 3E). In the next step, EDC-NHS was immobilized on the Fe:Ni(1:1)/C_GCE through incubation. During this step, the current signal decreased. The reason for this could be the surface crowding and repulsion of the $K_3[Fe(CN)_6]$ by the negative charge bearing functional groups of EDC-NHS.[14,18] In the next step, the EDC-NHS/Fe:Ni(1:1)/C_GCE was modified with anti-Lep. The anti-Lep modification showed further change in the CV signal. In the last step, BSA was added to minimize nonspecific binding.[16,19] The BSA/anti-Lep/EDC-NHS/Fe:Ni(1:1)/C_GCE showed the lowest current signal as expected. The Fe:Ni(1:3)/C and Fe:Ni(3:1)/C materials were modified following similar protocols. The electrode modification steps were also analyzed

https://doi.org/10.1021/acsbiomaterials.2c00642
ACS Biomater. Sci. Eng. XXXX, XXX, XXX−XXX

Table 1. Comparison of Lep Detection by the Proposed Sensors with Previously Reported Detection Methods[a]

sensor	methods	linear range (fg/mL)	LOD (fg/mL)	references
Fe:Ni(1:1)/C_GCE	EIS	500 to 8×10^7	157.4	this work
Fe:Ni(1:1)/C_SPCE	EIS	500 to 5×10^7	184.9	this work
$Au/Ce_3NbO_7/CeO_2$/SPE	DPV	500 to 1.2×10^7	138	8
BSA/antileptin/Glu/Cys/AuNPs/PG-BP/GCE	DPV	150 to 2.5×10^6	36	9
	ELISA	780 to 5×10^4	780	10
rGO-Au-ZZ-BNC	DPV	1 to 1×10^6	0.87	14
Fe_3O_4/PDA/Au	chemiluminescence	1×10 to 8×10^5	300	15
GWEs/PP/MIPL	EIS and conductance	1×10^6 to 3.2×10^7	1.1×10^5	17
Apt/Au NPs/TiO_2 NPs/SPE	EIS	1×10^3 to 1×10^6	312	18
GP electrode	EIS and CV	20 to 2×10^7	8.13	39

[a]SPE, screen printed electrode; Glu, glutaraldehyde; Cys, cysteamine; PG-BP, porous graphene functionalized black phosphorus; rGO, reduced graphene oxide; ZZ-BNC, bionanocapsule-ZZ; PDA, polydopamine; GWE, gold working electrode; PP, polyphenol; MIPL, molecularly imprinted polymer; GP, graphene.

with CV and EIS techniques (Figure S6). After each modification of the electrode, the impedance signal showed clear changes, indicating that the electrode surface underwent modification. The highest impedance was observed for BSA/anti-Lep/EDC-NHS/Fe:Ni/C_GCE.

The CV responses are shown in Figure 3G for 500 pg/mL of Lep in 5 mM $K_3[Fe(CN)_6]$ solution. Each of the FeNi/C materials showed distinct responses for the same concentration of Lep solution. The CV data showed that Lep/BSA/anti-Lep/EDC-NHS/Fe:Ni(1:1)/C_GCE had the smallest current response for the 500 pg/mL Lep solution. This change in current signal indicated that the Lep/BSA/anti-Lep/EDC-NHS/Fe:Ni(1:1)/C_GCE sensor had the most sensitive response toward low concentration Lep. EIS results for the Lep/BSA/anti-Lep/EDC-NHS/FeNi/C_GCE electrodes are shown in Figure 3H. The Fe:Ni(1:1)/C nanocomposite had the largest EIS signal for the Lep. From both CV and EIS, it was clear that Fe:Ni(1:1)/C material is the best candidate for Lep detection.

3.4. Optimization and Stability Checking of Fe:Ni (1:1)/C_GCE Sensor. Optimization of the incubation time and concentration of anti-Lep showed that 100 ng/mL of antibody is best suitable and 60 min is the optimized time period for anti-Lep immobilization, while for BSA, 90 min is the most suitable time period for BSA immobilization (Figure S7). The anti-Lep binding capability of the Fe:Ni(1:1)/C material was confirmed through SPR analysis.

The sensor modification process for SPR analysis is schematically shown in Figure 4A. Initially, the Fe:Ni(1:1)/C nanocomposite was dispersed in the EDC-NHS solution and was immobilized on the Au chip for preparing the nanocomposite modified Au chip (Figure 4A). After that, the EDC-NHS solution was passed over the sensor using the flow injector. The SPR sensorgram showed a good response around 150 s when the Fe:Ni(1:1)/C_Au sensor interacted with EDC-NHS (Figure 4B). It is likely that the −COOH group of the FeNi/C helped in this interaction.[37] After that, the anti-Lep solution was injected onto the EDC-NHS/Fe:Ni(1:1)/C_Au chip. This showed another change in the SPR sensorgram around 500 s (Figure 4B). This change in the sensorgram was due to the binding of the $-NH_2$ group of anti-Lep with the EDC-NHS.[38] The sensorgram showed a declining trend as over time the anti-Lep dissociated from the EDC-NHS/Fe:Ni(1:1)/C_Au sensor surface.[37] However, the sensorgram showed minimal change in its response over a time period of 500 s. This clearly indicated that the anti-Lep and EDC-NHS/Fe:Ni(1:1)/C interaction was steady.

3.5. Quantitative detection of Lep using FeNi/C_GCEs and FeNi/C_SPCEs LepSens. The performance of the LepSens for quantitative measurement of the Lep is studied using the EIS technique. In general, the normal Lep level in a human plasma sample is approximately ∼20 ng/mL.[11] In obese humans, the level of the Lep can reach up to ∼100 ng/mL, while the content in human adipose tissue under obese conditions varies from 17.6 to 20 ng/mL.[11,12] The proposed LepSens sensor was tested to see if it could accurately sense Lep hormone and what is the limit of detection (LOD) of the sensor for Lep. The electrode modification and Lep detection process are shown in Figure 4C. Figure 4D shows the EIS plots of the modified sensor obtained for several concentrations of Lep ranging from 500 fg/mL up to 100 ng/mL. It can be seen that the R_{ct} of each of the electrodes increases proportionally with increasing the level of Lep in solution up to 80 ng/mL. The corresponding calibration plots represented in Figure 4E show a linear relationship between the obtained R_{ct} with Lep concentration indicating that the sensor has a large concentration range for Lep. The R^2 value indicates a better fitting for the calibration plot. The value of LOD is calculated using the slope of the calibration and it is obtained to be only 157.4 fg/mL, which is sufficiently small for identifying Lep deficiency in the human body. Additionally, the sensor is highly effective for identifying obese conditions under an experimental setup.

To check the efficacy of the LepSens for detecting Lep in an integrated three-electrode system, we also tested it using an SPCE electrode instead of GCE. Figure 4F shows the EIS plots obtained for different concentrations of Lep (500 fg/mL to 80 ng/mL) using SPCE. The value of impedance of the LepSens increased linearly with Lep concentration; however, it was not that even as observed when GCE was used as the base substrate. The calibration plot (Figure 4G) shows that the value of R_{ct} is linear up to a 50 ng/mL concentration of Lep. The calculated LOD for this SPCE based Lep sensor was obtained to be approximately 184.9 fg/mL, indicating that the sensor functions perfectly for sensing Lep deficiency and obese conditions regardless of the base substrate. Table 1 shows how the proposed LepSens functions compared to the previously reported Lep sensors. Based on linear range and LOD, the LepSens has a higher potential of detecting Lep compared to the previously reported Lep sensors as shown in the table.

https://doi.org/10.1021/acsbiomaterials.2c00642
ACS Biomater. Sci. Eng. XXXX, XXX, XXX−XXX

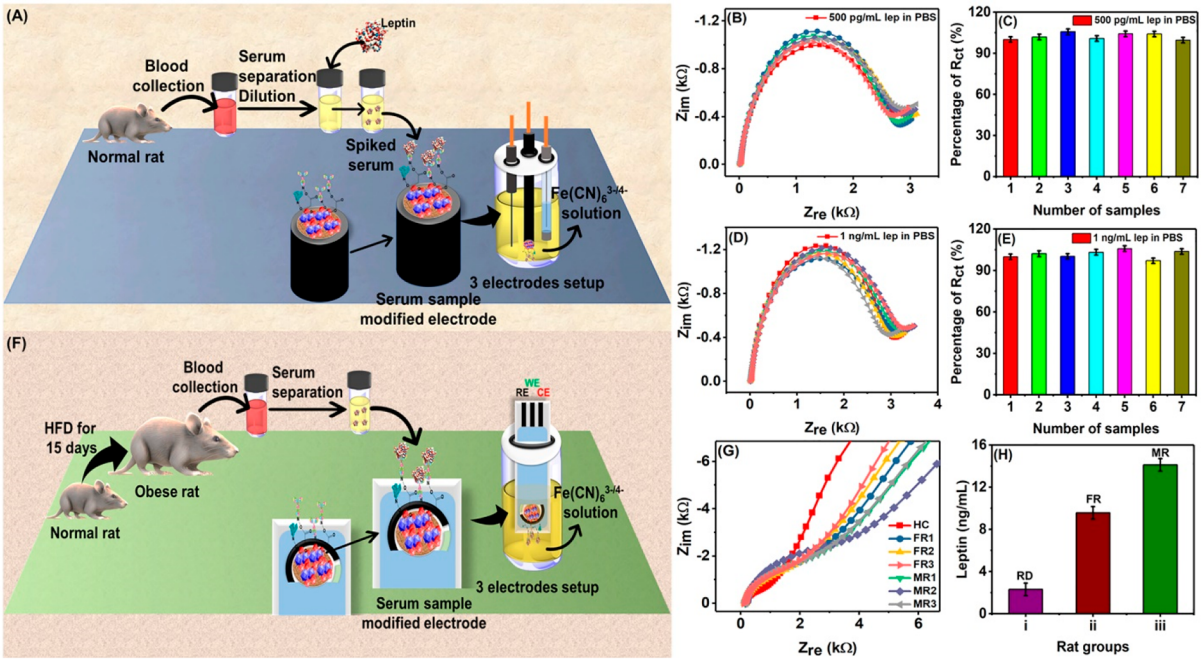

Figure 5. Rat serum sample analysis using the proposed LepSens. (A) Scheme showing the stepwise preparation of the spiked serum sample obtained from RD rats and subsequent sensor preparation using GCE. B and C show the EIS plots obtained for the RD rat serum samples. The serum samples are diluted and spiked with 500 pg/mL and 1 ng/mL Lep protein. D and E show the percentage of R_{ct} vs the number of serum sample plots for both concentrations. (F) Schematic illustration of the analysis of the whole serum samples obtained from HFD rats by using the SPCE based sensor. G shows the EIS plots obtained in whole HFD serum analysis. H shows the plot of Lep vs rat groups (RD = healthy control, FR = female rat, MR = male rat) obtained by analyzing EIS plots represented in G. Data were plotted as mean ± SEM, where n = 3.

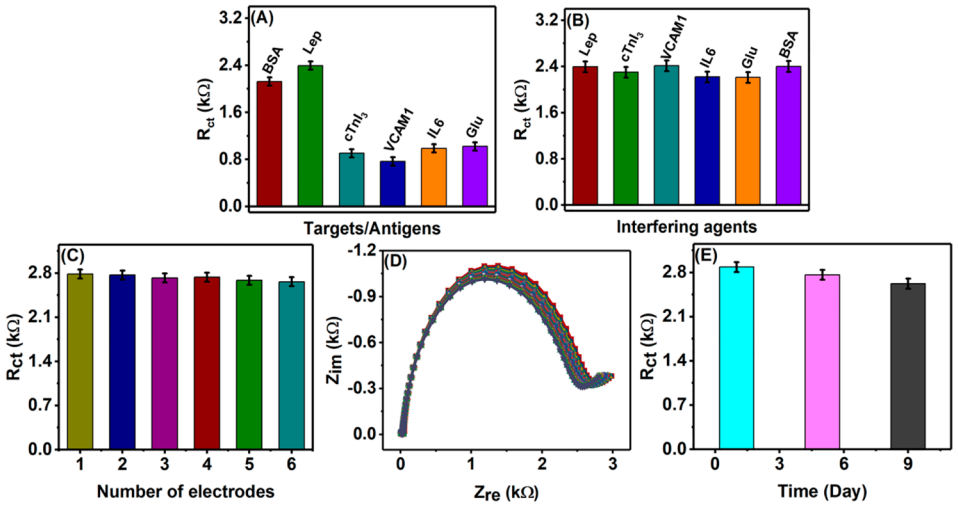

Figure 6. Selectivity and sensitivity of the LepSens were studied in the presence of interfering agents. Also, stability, reproducibility, and storage stability of the sensor are studied using the EIS technique. A shows the response of interfering substances ($cTnI_3$, VCAM1, IL6, and glucose) when compared with the Lep response. The bar plot for BSA indicates the signal for completion of electrode modification. B shows the value of R_{ct} obtained for Lep when both Lep and an interfering substance are individually taken together. C shows the EIS response of six GCE electrodes. D shows 30 consecutive EIS plots of the sensor, and E shows the stability of the sensor after 9 days of storing in 4 °C. Data was plotted as mean ± SEM, where n = 3.

3.6. Lep Detection from Serum Sample Using LepSens. For serum analysis, two groups of rats (six HFD rats and six RD rats) were considered. The body weight and body length of rats increased dramatically after the 15 day period. Once the obese model was created, the animals were euthanized to collect the blood followed by separation of serum by centrifugation. The process of sample collection and preparation for electrochemical detection is shown in Figure 5A for GCE. Before the analysis, the serum samples of the RD rats were diluted 100 times and spiked with two different concentrations of Lep (500 pg/mL and 1 ng/mL). Figure 5B and C exhibit the EIS responses of the six serum samples with two different concentrations and the result are compared with the EIS data obtained for Lep solution prepared in normal PBS. It can be seen that all electrodes resulted in comparable R_{ct} values for both concentrations. The percentage of R_{ct} vs

https://doi.org/10.1021/acsbiomaterials.2c00642
ACS Biomater. Sci. Eng. XXXX, XXX, XXX−XXX

number of the serum sample plots represented in Figure 5D and E demonstrated that the standard deviation for each of the electrode is within 5%. This finding indicates that the LepSens is efficient and capable for sensitive detection of Lep from biological sample. Next, the whole serum samples collected from HFD rats were utilized to construct the modified SPCE electrode. Figure 5G exhibits the EIS responses of the HFD serum samples obtained from female and male rats (FR and MR), and the responses were compared with the RD serum response. Figure 5H shows the bar plot representing the resultant Lep in nanograms per liter obtained by using the SPCE based immunosensor. The normal level of Lep obtained from HC (healthy control, RD rats) serum was within the range of 2.3 ng/mL, which is comparable with the previously reported Lep level under normal conditions.[40,41] The HFD rat serum analysis by the proposed LepSens resulted in a significant increment of the Lep level in FRs (~9.57 ng/mL) and MRs (~14 ng/mL), which confirms the sensor's utility and effectiveness for real-time detection of Lep for diagnosing leptin resistance.

3.7. Selectivity, Anti-Interference Ability, Stability, and Reproducibility. The electrochemical biosensors need to be able to selectively identify the target analyte in the presence of interfering species. That is why we have tested the selectivity of the LepSens (Lep/BSA/anti-Lep/EDC-NHS/Fe:Ni(1:1)/C_GCEs) with the following compounds: $cTnI_3$, VCAM1, IL6, glucose, and BSA. A selectivity test was carried out by modifying each electrode with Lep (100 pg/mL), $cTnI_3$ (5 ng/mL), VCAM1 (5 ng/mL), IL6 (5 ng/mL), and glucose (0.02 g/mL). The interfering species concentration was taken to be at least 50 times higher than Lep concentration. Figure 6A shows that the R_{ct} value for the Lep modified electrode was much higher compared to those of the $cTnI_3$, VCAM1, IL6, and glucose electrodes. This experiment was repeated three times to ensure the selectivity of the Lep/BSA/anti-Lep/EDC-NHS/Fe:Ni(1:1)/C_GCEs.

The biological samples are complex systems where different chemicals are present together with Lep. We performed the anti-interference test by taking Lep with different interfering species in the same solution (Figure 6B). The results from Figure 6B shows that the R_{ct} value did not change much when Lep was taken with different interfering species. This study demonstrates that the sensor is Lep specific and the signal does not alter much upon taking interfering species in the same solution.

The reproducibility test for the Lep/BSA/anti-Lep/EDC-NHS/Fe:Ni(1:1)/C_ SPCE was done by modifying six different GCEs following similar conditions. Figure 6C shows the data for the reproducibility test. The results indicate that the biosensor fabrication process is highly reproducible.

The experimental stability and storage stability of the Lep/BSA/anti-Lep/EDC-NHS/Fe:Ni(1:1)/C_ SPCE was also tested. Thirty EIS experiments were done using the same modified biosensor for determining its experimental stability. Figure 6D shows that the LepSens had excellent experimental stability even after 30 EIS runs. The storage stability was tested for 9 days, and the results are shown in Figure 6E. The Lep/BSA/anti-Lep/EDC-NHS/Fe:Ni(1:1)/C_SPCE retained almost 89.5% performance on day 9 compared to day 1. This shows good storage stability of the Lep biosensors.

4. CONCLUSIONS

This report represents an impedimetric immunosensing platform for the selective detection of Lep using a heterometallic nanocomposite-based tool from the serum sample. The characteristics profile demonstrated that the synthesized Fe:Ni/C material consisted of both Fe and Ni supported by the carbon base. Out of the three compositions, the Fe:Ni(1:1)/C showed the best response for Lep detection. The SPR sensorgram confirmed stable binding between anti-Lep and the nanocomposite having equal ratios of Fe and Ni. The applicability of the LepSense for detecting Lep was studied with two different electrodes to determine whether the sensor could function adequately regardless of the type of base electrodes. The linear range for Lep detection was found to be 500 fg/mL to 50 ng/mL with a LOD of 184.9 fg/mL for SPCEs. The wide linear range that encompasses the physiological Lep concentration for humans indicates that the proposed LepSens could be used for Lep detection from clinical samples. The LepSens were able to detect Lep from rat serum samples with very good accuracy. The excellent selectivity and anti-interference ability with very good stability and reproducibility indicate that the Fe:Ni/C has excellent catalytic activity toward Lep detection, and the FeNi/C coated SPCEs could be used for point-of-care Lep detection.

■ ASSOCIATED CONTENT

Supporting Information

The Supporting Information is available free of charge at https://pubs.acs.org/doi/10.1021/acsbiomaterials.2c00642.

XPS survey spectrum; CV response of GCE, FeNi(1:1)/C_GCE, FeNi(1:3)/C_GCE, and FeNi(3:1)/C_GCE; consecutive CV responses of FeNi(3:1)/C_GCE; scan rate variation data; 50 consecutive CVs for stability; electrochemical analysis of the layer-by-layer modifications; optimization of the time period and the concentration (PDF)

■ AUTHOR INFORMATION

Corresponding Authors

Juan C. Noveron − *Department of Chemistry, University of Texas at El Paso, El Paso, Texas 79968, United States;* orcid.org/0000-0002-2762-7802; Phone: 915-747-7572; Email: jcnoveron@utep.edu

Md Nurunnabi − *Department of Pharmaceutical Sciences, School of Pharmacy, University of Texas at El Paso, El Paso, Texas 79902, United States; Aerospace Center (cSETR) and Biomedical Engineering, College of Engineering, University of Texas at El Paso, El Paso, Texas 79965, United States;* orcid.org/0000-0003-4457-3401; Phone: 915-747-8335; Email: mnurunnabi@utep.edu

Authors

Tamanna Islam − *Department of Pharmaceutical Sciences, School of Pharmacy, University of Texas at El Paso, El Paso, Texas 79902, United States*

Md Ariful Ahsan − *Department of Chemistry, University of Texas at El Paso, El Paso, Texas 79968, United States;* orcid.org/0000-0002-2024-8690

Masud Hassan − *Global Centre for Environmental Remediation, College of Engineering, Science and Environment, University of Newcastle, Callaghan, New South Wales 2308, Australia;* orcid.org/0000-0001-6271-6344

https://doi.org/10.1021/acsbiomaterials.2c00642
ACS Biomater. Sci. Eng. XXXX, XXX, XXX−XXX

Humayra Afrin − *Department of Pharmaceutical Sciences, School of Pharmacy, University of Texas at El Paso, El Paso, Texas 79902, United States;* orcid.org/0000-0002-2720-1369

Jaqueline Pena-Zacarias − *Biological Sciences Program, College of Science, University of Texas at El Paso, El Paso, Texas 79902, United States*

Ali Aldalbahi − *Department of Chemistry, College of Science, King Saud University, Riyadh 11451, Saudi Arabia;* orcid.org/0000-0003-1644-2367

Bonifacio Alvarado-Tenorio − *Instituto de Ciencias Biomédicas, Universidad Autónoma de Ciudad Juárez, Ciudad Juárez, Chihuahua 32315, Mexico*

Complete contact information is available at: https://pubs.acs.org/10.1021/acsbiomaterials.2c00642

Author Contributions

♦These authors contributed equally to this work.

Author Contributions

T.A., M.A.A., J.C.N., and M.N. have designed the project. T.A., M.A.A., M.H., H.A., J.P.Z., A.A., and B.A.T. have conducted the experiments. The manuscript was written through contributions of all authors. All authors have given approval to the final version of the manuscript.

Notes

The authors declare the following competing financial interest(s): A provisional patent application (Application # 63/370,147) was filed on August 2, 2022, where M.N., M.A.A., J.C.N., and T.A. are listed as inventors.

■ ACKNOWLEDGMENTS

We acknowledge funding by Cancer Prevention Research Institute of Texas (CPRIT) through Texas Regional Excellence in Cancer Award (TREC) under Award No. PR210153. Research reported in this publication was also supported by the Lizanell Colbert Colwell Foundation. This research was funded in part by the U.S. National Science Foundation (NSF) Nanotechnology-Enabled Water Treatment Center (NEWT ERC435 1449500; to J.C.N.) and the USDA 2019-38422-30214 (to J.C.N.). The Ralph & Kathleen Ponce de Leon Professorship to J.C.N is gratefully acknowledged. We would like to thank Dr. Huiming Zhang and Dr. Yun Lin (EMX unit, University of Newcastle, Australia) for assistance of the microscopic characterization of the materials. The authors also acknowledge the King Saud University, Riyadh, Saudi Arabia, for funding this work through Researchers Supporting Project number (RSP-2021/30).

■ REFERENCES

(1) Yu, W.; Rohli, K. E.; Yang, S.; Jia, P. Impact of Obesity on COVID-19 Patients. *J. Diabetes Complications* **2021**, *35* (3), 107817.

(2) Palaiodimos, L.; Kokkinidis, D. G.; Li, W.; Karamanis, D.; Ognibene, J.; Arora, S.; Southern, W. N.; Mantzoros, C. S. Severe Obesity Is Associated with Higher In-Hospital Mortality in a Cohort of Patients with COVID-19 in the Bronx, New York. *Metabolism.* **2020**, *108*, 154262.

(3) Weihrauch-Blüher, S.; Wiegand, S. Risk Factors and Implications of Childhood Obesity. *Curr. Obes. Rep.* **2018**, *7* (4), 254−259.

(4) Włodarczyk, M.; Nowicka, G. Obesity, DNA Damage, and Development of Obesity-Related Diseases. *Int. J. Mol. Sci.* **2019**, *20* (5), 1146.

(5) Fang, X.; Wang, X.; Song, Z.; Han, D.; Yin, X.; Liu, B.; Chen, L.; Zhang, R.; Lian, F.; Sui, X. Causal Association of Childhood Obesity with Cancer Risk in Adulthood: A Mendelian Randomization Study. *Int. J. Cancer* **2021**, *149* (7), 1421−1425.

(6) Ostrand-Rosenberg, S. Myeloid-Derived Suppressor Cells: Facilitators of Cancer and Obesity-Induced Cancer. *Annu. Rev. Cancer Biol.* **2021**, *5*, 17−38.

(7) Islam, T.; Huda, M. N.; Ahsan, M. A.; Afrin, H.; Joseph J Salazar, C.; Nurunnabi, M. Theoretical and Experimental Insights into the Possible Interfacial Interactions between β-Glucan and Fat Molecules in Aqueous Media. *J. Phys. Chem. B* **2021**, *125* (50), 13730−13743.

(8) Liu, X.; Tseng, C. L.; Lin, L. Y.; Lee, C. A.; Li, J.; Feng, L.; Song, L.; Li, X.; He, J. H.; Sakthivel, R.; Chung, R. J. Template-Free Synthesis of Mesoporous Ce3NbO7/CeO2 Hollow Nanospheres for Label-Free Electrochemical Immunosensing of Leptin. *Sensors Actuators, B Chem.* **2021**, *341* (April), 130005.

(9) Cai, J.; Gou, X.; Sun, B.; Li, W.; Li, D.; Liu, J.; Hu, F.; Li, Y. Porous Graphene-Black Phosphorus Nanocomposite Modified Electrode for Detection of Leptin. *Biosens. Bioelectron.* **2019**, *137*, 88−95.

(10) Imagawa, K.; Matsumoto, Y.; Numata, Y.; Morita, A.; Kikuoka, S.; Tamaki, M.; Higashikubo, C.; Tsuji, T.; Sasakura, K.; Teraoka, H.; Masuzaki, H.; Hosoda, K.; Ogawa, Y.; Nakao, K. Development of a Sensitive ELISA for Human Leptin, Using Monoclonal Antibodies. *Clin. Chem.* **1998**, *44* (10), 2165−2171.

(11) Wada, N. *Leptin*; Elsevier Inc., 2016; Vol. *306*. DOI: 10.1016/B978-0-12-801028-0.00380-9.

(12) Prokop, J. W.; Duff, R. J.; Ball, H. C.; Copeland, D. L.; Londraville, R. L. Leptin and Leptin Receptor: Analysis of a Structure to Function Relationship in Interaction and Evolution from Humans to Fish. *Peptides* **2012**, *38* (2), 326−336.

(13) Gruzdeva, O.; Borodkina, D.; Uchasova, E.; Dyleva, Y.; Barbarash, O. Leptin Resistance: Underlying Mechanisms and Diagnosis. *Diabetes, Metab. Syndr. Obes. Targets Ther.* **2019**, *12*, 191−198.

(14) Zhang, C.; Liu, L.; Li, H.; Hu, J.; Zhang, J.; Zhou, H.; Zhang, Z.; Du, X. An Oriented Antibody Immobilization Based Electrochemical Platform for Detection of Leptin in Human with Different Body Mass Index. *Sensors Actuators B Chem.* **2022**, *353* (xxxx), 131074.

(15) He, Y.; Sun, J.; Wang, X.; Wang, L. Detection of Human Leptin in Serum Using Chemiluminescence Immunosensor: Signal Amplification by Hemin/G-Quadruplex DNAzymes and Protein Carriers by Fe3O4/Polydopamine/Au Nanocomposites. *Sensors Actuators, B Chem.* **2015**, *221*, 792−798.

(16) Islam, T.; Hasan, M. M.; Awal, A.; Nurunnabi, M.; Ahammad, A. J. S. Metal Nanoparticles for Electrochemical Sensing: Progress and Challenges in the Clinical Transition of Point-of-Care Testing. *Molecules* **2020**, *25*, 5787.

(17) Mihailescu, C. M.; Stan, D.; Savin, M.; Moldovan, C. A.; Dinulescu, S.; Radulescu, C. H.; Firtat, B.; Muscalu, G.; Brasoveanu, C.; Ion, M.; Dragomir, D.; Stan, D.; Ion, A. C. Platform with Biomimetic Electrochemical Sensors for Adiponectin and Leptin Detection in Human Serum. *Talanta* **2020**, *210*, 120643.

(18) Erkmen, C.; Tiğ, G. A.; Uslu, B. First Label-Free Impedimetric Aptasensor Based on Au NPs/TiO2 NPs for the Determination of Leptin. *Sensors Actuators B Chem.* **2022**, *358*, 131420.

(19) Madhurantakam, S.; Babu, K. J.; Rayappan, J. B. B.; Krishnan, U. M. Nanotechnology-Based Electrochemical Detection Strategies for Hypertension Markers. *Biosens. Bioelectron.* **2018**, *116* (May), 67−80.

(20) Ahsan, M. A.; Puente Santiago, A. R.; Hong, Y.; Zhang, N.; Cano, M.; Rodriguez-Castellon, E.; Echegoyen, L.; Sreenivasan, S. T.; Noveron, J. C. Tuning of Trifunctional NiCu Bimetallic Nanoparticles Confined in a Porous Carbon Network with Surface Composition and Local Structural Distortions for the Electrocatalytic Oxygen Reduction, Oxygen and Hydrogen Evolution Reactions. *J. Am. Chem. Soc.* **2020**, *142* (34), 14688−14701.

(21) Hasan, M. M.; Islam, T.; Ratan, Z. A.; Shaikh, M. N.; Karim, M. R.; Rahman, M. M.; Alharbi, H. F.; Uddin, J.; Aziz, M. A.; Ahammad, A. J. S. Ni and Co Oxide Water Oxidation Electrocatalysts: Effect of

Thermal Treatment on Catalytic Activity and Surface Morphology. *Renew. Sustain. Energy Rev.* **2021**, *145*, 111097.
(22) Samad, S.; Loh, K. S.; Wong, W. Y.; Sudarsono, W.; Lee, T. K.; Wan Daud, W. R. Effect of Various Fe/Co Ratios and Annealing Temperatures on a Fe/Co Catalyst Supported with Nitrogen-Doped Reduced Graphene Oxide towards the Oxygen Reduction Reaction. *J. Alloys Compd.* **2020**, *816*, 152573.
(23) Ahsan, M. A.; Imam, M. A.; Puente Santiago, A. R.; Rodriguez, A.; Alvarado-Tenorio, B.; Bernal, R.; Luque, R.; Noveron, J. C. Spent Tea Leaves Templated Synthesis of Highly Active and Durable Cobalt-Based Trifunctional Versatile Electrocatalysts for Hydrogen and Oxygen Evolution and Oxygen Reduction Reactions. *Green Chem.* **2020**, *22* (20), 6967−6980.
(24) Ding, R.; Chen, Q.; Luo, Q.; Zhou, L.; Wang, Y.; Zhang, Y.; Fan, G. Salt Template-Assisted: In Situ Construction of Ru Nanoclusters and Porous Carbon: Excellent Catalysts toward Hydrogen Evolution, Ammonia-Borane Hydrolysis, and 4-Nitrophenol Reduction. *Green Chem.* **2020**, *22* (3), 835−842.
(25) Lei, Z. D.; Xue, Y. C.; Chen, W. Q.; Li, L.; Qiu, W. H.; Zhang, Y.; Tang, L. The Influence of Carbon Nitride Nanosheets Doping on the Crystalline Formation of MIL-88B(Fe) and the Photocatalytic Activities. *Small* **2018**, *14* (35), 1802045.
(26) Chu, M.; Chen, C.; Guo, W.; Lu, L.; Wu, Y.; Wu, H.; He, M.; Han, B. Enhancing Electroreduction of CO2 over Bi2WO6 Nanosheets by Oxygen Vacancies. *Green Chem.* **2019**, *21* (10), 2589−2593.
(27) Su, Y.; Jiang, H.; Zhu, Y.; Yang, X.; Shen, J.; Zou, W.; Chen, J.; Li, C. Enriched Graphitic N-Doped Carbon-Supported Fe3O4 Nanoparticles as Efficient Electrocatalysts for Oxygen Reduction Reaction. *J. Mater. Chem. A* **2014**, *2* (20), 7281−7287.
(28) Jeon, I. Y.; Zhang, S.; Zhang, L.; Choi, H. J.; Seo, J. M.; Xia, Z.; Dai, L.; Baek, J. B. Edge-Selectively Sulfurized Graphene Nanoplatelets as Efficient Metal-Free Electrocatalysts for Oxygen Reduction Reaction: The Electron Spin Effect. *Adv. Mater.* **2013**, *25* (42), 6138−6145.
(29) Ahsan, M. A.; Puente Santiago, A. R.; Rodriguez, A.; Maturano-Rojas, V.; Alvarado-Tenorio, B.; Bernal, R.; Noveron, J. C. Biomass-Derived Ultrathin Carbon-Shell Coated Iron Nanoparticles as High-Performance Tri-Functional HER, ORR and Fenton-like Catalysts. *J. Clean. Prod.* **2020**, *275*, 124141.
(30) Xiang, J.; Li, J.; Zhang, X.; Ye, Q.; Xu, J.; Shen, X. Magnetic Carbon Nanofibers Containing Uniformly Dispersed Fe/Co/Ni Nanoparticles as Stable and High-Performance Electromagnetic Wave Absorbers. *J. Mater. Chem. A* **2014**, *2* (40), 16905−16914.
(31) Oukil, D.; Makhloufi, L.; Saidani, B. Preparation of Polypyrrole Films Containing Ferrocyanide Ions Deposited onto Thermally Pre-Treated and Untreated Iron Substrate: Application in the Electroanalytical Determination of Ascorbic Acid. *Sensors Actuators, B Chem.* **2007**, *123* (2), 1083−1089.
(32) Cheng, Y.; Wu, X.; Veder, J. P.; Thomsen, L.; Jiang, S. P.; Wang, S. Tuning the Electrochemical Property of the Ultrafine Metal-Oxide Nanoclusters by Iron Phthalocyanine as Efficient Catalysts for Energy Storage and Conversion. *Energy Environ. Mater.* **2019**, *2* (1), 5−17.
(33) Ramadoss, A.; Kang, K. N.; Ahn, H. J.; Kim, S. I.; Ryu, S. T.; Jang, J. H. Realization of High Performance Flexible Wire Supercapacitors Based on 3-Dimensional NiCo2O4/Ni Fibers. *J. Mater. Chem. A* **2016**, *4* (13), 4718−4727.
(34) Yang, P.; Wu, Z.; Jiang, Y.; Pan, Z.; Tian, W.; Jiang, L.; Hu, L. Fractal (NixCo1−x)9Se8 Nanodendrite Arrays with Highly Exposed (01$\bar{1}$) Surface for Wearable, All-Solid-State Supercapacitor. *Adv. Energy Mater.* **2018**, *8* (26), 1801392.
(35) Fayad, R.; Dhainy, J.; Ghandour, H.; Halaoui, L. Electrochemical Study of the Promoting Effect of Fe on Oxygen Evolution at Thin "NiFe-Bi" Films and the Inhibiting Effect of Al in Borate Electrolyte. *Catal. Sci. Technol.* **2017**, *7* (17), 3876−3891.
(36) Ahammad, A. J. S.; Pal, P. R.; Shah, S. S.; Islam, T.; Mahedi Hasan, M.; Qasem, M. A. A.; Odhikari, N.; Sarker, S.; Kim, D. M.; Abdul Aziz, M. Activated Jute Carbon Paste Screen-Printed FTO Electrodes for Nonenzymatic Amperometric Determination of Nitrite. *J. Electroanal. Chem.* **2019**, *832*, 368−379.
(37) Zhu, H.; Lu, Y.; Xia, J.; Liu, Y.; Chen, J.; Lee, J.; Koh, K.; Chen, H. Aptamer-Assisted Protein Orientation on Silver Magnetic Nanoparticles: Application to Sensitive Leukocyte Cell-Derived Chemotaxin 2 Surface Plasmon Resonance Sensors. *Anal. Chem.* **2022**, *94* (4), 2109−2118.
(38) Choi, J. U.; Zhang, X.; Hasan, M. M.; Karim, M.; Chung, S. W.; Alam, F.; Alqahtani, F.; Reddy, S. Y.; Kim, I.-S.; Al-Hilal, T. A.; Byun, Y. Biomaterials Targeting Angiogenic Growth Factors Using Therapeutic Glycosaminoglycans on Doppel-Expressing Endothelial Cells for Blocking Angiogenic Signaling in Cancer. *Biomaterials* **2022**, *283*, 121423.
(39) Özcan, B.; Sezgintürk, M. K. A Novel and Disposable GP-Based Impedimetric Biosensor Using Electropolymerization Process with PGA for Highly Sensitive Determination of Leptin: Early Diagnosis of Childhood Obesity. *Talanta* **2021**, *225*, 121985.
(40) Chen, G.; Koyama, K.; Yuan, X.; Lee, Y.; Zhou, Y. T.; O'Doherty, R.; Newgard, C. B.; Unger, R. H. Disappearance of Body Fat in Normal Rats Induced by Adenovirus-Mediated Leptin Gene Therapy. *Proc. Natl. Acad. Sci. U. S. A.* **1996**, *93* (25), 14795−14799.
(41) Engelbregt, M. J. T.; Van Weissenbruch, M. M.; Popp-Snijders, C.; Lips, P.; Delemarre-Van de Waal, H. A. Body Mass Index, Body Composition, and Leptin at Onset of Puberty in Male and Female Rats after Intrauterine Growth Retardation and after Early Postnatal Food Restriction. *Pediatr. Res.* **2001**, *50* (4), 474−478.

https://doi.org/10.1021/acsbiomaterials.2c00642
ACS Biomater. Sci. Eng. XXXX, XXX, XXX−XXX